

CHAPTER 6

Tidal Computations for the Yellow Sea

Byung Ho Choi*

Abstract

A two-dimensional numerical model of the Yellow Sea has been used to compute cotidal and coamplitude charts and harmonic constants of tidal currents for the four major tidal constituents M_2 , S_2 , K_1 , O_1 tides in the region with the mesh resolution of $1/5$ degree latitude by $1/4$ degree longitude finite difference grid system. An additional model incorporating dynamical grid nesting procedure which employs a one-third grid refinement scheme was also used to reproduce the M_2 tidal regime in more detailed resolution for the part of west coast of Korea where extensive coastal development including potential tidal power and land reclamation scheme is concerned. Comparisons between observations and model result have been carried out based on coastal gauges and moored current meter data. Reasonable agreement was found between observations and model results, thus supporting the computed distribution of tides in the region. It was also shown that the dynamically linked model particularly well within 5% in amplitude and 5 degrees in phase of observed M_2 tide in the refined mesh region of the west coast of Korea.

Introduction

The tidal phenomena of the Yellow Sea are extremely complex. During the late 1920's and early 1930's extensive studies of this shelf sea area were reported and a considerable number of tidal measurements were made, from which cotidal and corange charts of diurnal and semidiurnal tides were prepared (Ogura, 1933). Russian workers (Boris, 1958; Tsiklauri et al., 1961; Stepanov et al., 1964) reported the first application of two-dimensional mathematical models on the one hand to the Yellow Sea and on the other hand, to the Gulfs of Pohai and Liautung, employing boundary value method which calls for much tidal data at external boundary points along the coast and open boundary. While the latter models were satisfactorily used to reproduce the M_2 and K_1 tides in the Gulfs of Liautung and Pohai where extensive tidal data exists, the Yellow Sea model was only used to test the sensitivity of the tides of that area to changes in the boundary tidal input data, depths along the boundaries and Coriolis parameter. Their results indicated that the computed tides in the Yellow Sea were highly sensitive to even small changes in levelling data and the depths along the boundaries.

During the past few years series of numerical tidal models (An, 1977; Choi, 1980; Shen, 1980; Xia and Wang, 1984) based on initial value method have been reported and it was demonstrated by these models that the tides

*Professor, Dept. of Civil Eng., Sung Kyun Kwan University, Suwon Campus Korea.

can be satisfactorily reproduced, thus providing general information on the tidal dynamics in this sea area. However improvement on the accuracy of the model and verification of computed tidal currents were much limited due to the lack of long-term tidal observations.

In the present paper, an initial attempt is made to provide separate tidal charts of four major M_2 , S_2 , K_1 and O_1 tides in the Yellow Sea from the numerical model and comparisons between model results and the observations including recently available current meter data were described. Further effort to reproduce the tides in western Yellow Sea in more detailed manner by adopting the mesh-connecting scheme for the purpose of assessing the tidal modification due to coastal development is also included.

Numerical Model

Considering the area covered by the model, the curvature of the earth and the variation with latitude of the Coriolis acceleration are taken into account by adopting spherical coordinates. The equations of motion and continuity as used in this model are (Flather, 1976):

$$\frac{1}{R \cos \phi} \left\{ \frac{\partial}{\partial \chi} (Hu) + \frac{\partial}{\partial \phi} (Hv \cos \phi) \right\} + \frac{\partial \xi}{\partial t} = 0, \quad (1)$$

$$\frac{\partial u}{\partial t} + \frac{u}{R \cos \phi} \frac{\partial u}{\partial \chi} + \frac{v}{R} \frac{\partial u}{\partial \phi} - \frac{uv \tan \phi}{R} - 2\omega \sin \phi v + \frac{k_b u \sqrt{u^2 + v^2}}{H} + \frac{g}{R \cos \phi} \frac{\partial \xi}{\partial \chi} = 0, \quad (2)$$

$$\frac{\partial v}{\partial t} + \frac{u}{R \cos \phi} \frac{\partial v}{\partial \chi} + \frac{v}{R} \frac{\partial v}{\partial \phi} + \frac{u^2 \tan \phi}{R} + 2\omega \sin \phi u + \frac{k_b v \sqrt{u^2 + v^2}}{H} + \frac{g}{R} \frac{\partial \xi}{\partial \phi} = 0, \quad (3)$$

Equations (1) - (3) are vertically integrated hydrodynamical equations where the notation is

t	time
χ, ϕ	east-longitude and latitude respectively
ξ	elevation of the sea surface above the undisturbed depth
h	undisturbed depth of water
$H = h + \xi$	total depth of water
R	the radius of the Earth
ω	angular speed of the Earth's rotation
g	acceleration due to gravity
k_b	coefficient of bottom friction
u', v'	components of current in the directions of χ, ϕ respectively at a depth z below the undisturbed sea level
u, v	components of depth-mean current given by
	$u = \frac{1}{h+\xi} \int_{-h}^{\xi} u'(z) dz, \quad v = \frac{1}{h+\xi} \int_{-h}^{\xi} v'(z) dz$

These equations, formulated with a quadratic law of bottom friction, are integrated on a staggered finite difference grid using the scheme described by Roberts and Weiss (1967) which centers the advective terms in time and space. The method employed for implementing this scheme is described by Flather and Heaps (1975) and Flather (1976).

Initial and boundary condition required for the solution of equations (1) to (3) are as follows:

$$\text{At } t = 0 : u(x, \phi, t), v(x, \phi, t) \text{ and } \xi(x, \phi, t)$$

are specified for all positions at which the equations are to be solved. At a land boundary: the component of the flow normal to the boundary is permanently zero:

$$u \cos \theta + v \sin \theta = 0$$

where θ is the angle between the normal to the coast directed out of the sea region and X axis. Therefore

- $u = 0$ is the boundary condition at a ϕ -directed land boundary
- $v = 0$ is the boundary condition at a X -directed land boundary.

Along an open boundary, elevation is specified as a function of time and position along the boundary: $\xi(X, \phi, t)$ is supplied.

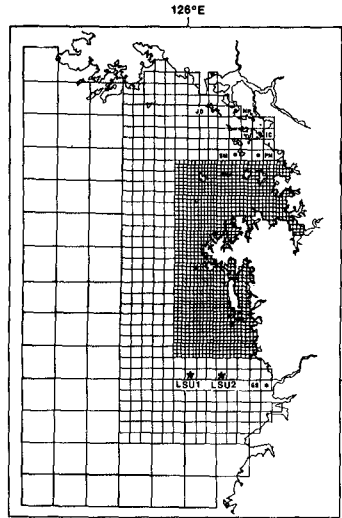
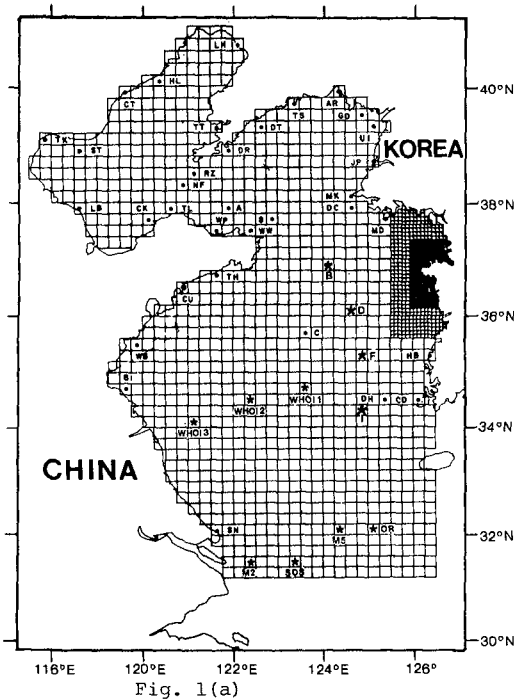


Fig. 1. Finite difference grid system of the Yellow Sea model.

In shallow sea areas provision is made in the numerical scheme for representing the drying of tidal flats.

The three different grid systems of the model are shown in Fig. 1. The coarse mesh has a grid resolution of 1/5 degree latitude by 1/4 degree longitude and this coarse grid has been used to compute overall tidal distribution in the Yellow Sea. This is the same grid spacing as that used in the two-dimensional shelf model of Choi (1980). The mesh size of intermediate grid system is one-third of this (1/15 degree latitude by 1/12 degree longitude) and a fine mesh system resulting from another refinement to provide a resolution of 1/45 degree latitude by 1/36 degree longitude. The dynamically linkaged model interconnecting three different grid systems has been used to compute the M₂ tidal regime of the west coast of Korea in detailed resolution.

In the model three different values of frictional parameters (0.0025 for the coarse grid and 0.0028, 0.0030 for the intermediate and fine grids) were used to give the best results for the reproduction of the tides. The open boundaries of the model border the line of latitude 31.2 degree North from the entrance of Changjiang River and the line of longitude 126.5 degree East. The boundary elevations were specified as a function of position and time. To satisfy explicit stability conditions, a timestep of six minutes was used for the coarse grid model and a timestep of one lunar minute was used for the dynamically linkaged model. Time and phases referred to in this study are referenced to 135 degree east longitude (time zone, -9H).

The numerical scheme employed was described previously (Choi, 1980) and the dynamic grid nesting procedure for joining the different grid mesh is similar to those by Owen (1979). When a computation of a variable on the one grid system in the mesh connected area requires a variable on another grid system, a linearly interpolated value is used.

Fig. 2 shows the mesh refinement grid area between two different size of meshes which are connected with an one-third refinement scheme. The finite difference scheme, which advances ξ, u, v over the entire network at time t to obtain their values at time $t + \Delta t$ is explicit and changes its scanning direction for calculation of u, v at alternate time-steps. When calculation of u, v on one grid system in the connected region requires variables ξ, u, v 's on joining grid system, a linearly interpolated values were used.

Referring to Fig. 2(a) showing mesh refinement in u-direction, u-velocities in the fine grid region are calculated as:

$$u_{i,n-1} = \frac{1}{2}(u_{i,n} + \frac{1}{3}(2u_{i,l} + u_{i,m})) \quad (4)$$

$$u_{i,l} = \frac{1}{2}(u_{i,l} + u_{i,l})$$

$$u_{i,n-1} = \frac{1}{2}(u_{i,n} + \frac{1}{3}(2u_{i,l} + u_{i,m}))$$

The calculation of u in the coarse side of the connection requires

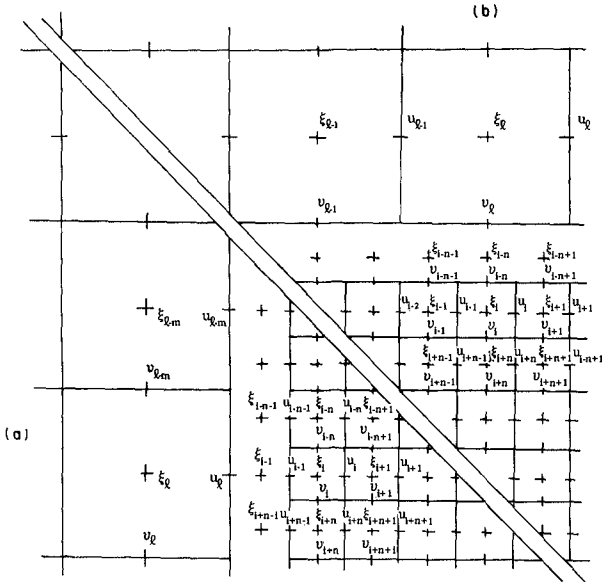


Fig. 2. Combination of two different grid system.

ξ values and v value in the fine mesh side:

$$\tilde{v} = \frac{1}{4}(v_{\xi-m} + v_{\xi} + v_{\xi+2n} + v_{\xi+n}) \quad (5)$$

$$\xi_{\xi+1} = \xi_i$$

Values of ξ along the connected regions are calculated as:

$$\xi_{i+n-1} = \frac{1}{3} \left(\frac{2}{3} \xi_{\xi} + \frac{1}{3} \xi_{\xi-m} \right) + \frac{2}{3} \xi_{i-n} \quad (6)$$

$$\xi_{i+1} = \frac{2}{3} \xi_i + \frac{1}{3} \xi_{\xi}$$

$$\xi_{i+n+1} = \frac{1}{3} \left(\frac{2}{3} \xi_{\xi} + \frac{1}{3} \xi_{\xi+m} \right) + \frac{2}{3} \xi_{i+n}$$

Referring to Fig. 2(b) showing mesh refinement in v -direction, v -velocities in fine grid region are calculated as:

$$v_{i+n-1} = \frac{1}{2} (v_{i-1} + \frac{1}{3} (2v_{\xi} + v_{\xi_1})) \quad (7)$$

$$v_{i+n} = \frac{1}{2} (v_{\xi} + v_i)$$

$$v_{i+n+1} = \frac{1}{2} (v_{i+1} + \frac{1}{3} (2v_{\xi} + v_{\xi_1}))$$

The calculation of v in the coarse side of the connection requires u values and ξ value in the fine mesh side:

$$\tilde{u} = \frac{1}{4} (u_{\xi_1} + u_{\xi} + u_{i-2} + u_{i+1}) \quad (8)$$

$$\xi_{\xi-m} = \xi_i$$

Values of ξ along the row of the connected region are calculated as:

$$\begin{aligned}\xi_{i+n-1} &= \frac{1}{3} \left(\frac{2}{3} \xi_{\ell} + \frac{1}{3} \xi_{\ell+1} \right) + \frac{2}{3} \xi_{i-1} \\ \xi_{i+n} &= \frac{2}{3} \xi_i + \frac{1}{3} \xi_{\ell} \\ \xi_{i+n+1} &= \frac{1}{3} \left(\frac{2}{3} \xi_{\ell} + \frac{1}{3} \xi_{\ell+1} \right) + \frac{2}{3} \xi_{i+1}\end{aligned}\quad (9)$$

Along the rows and columns of connected region of one grid space, non-linear advective terms were neglected to avoid excessive interpolations,

Model Results

Tidal Elevations

The dynamically linkaged model of which the grid system is shown in Fig. 1 was run for five tidal cycle cycles to achieve the stable tidal regime. Results of further sixth cycle was then analyzed to yield M_2 tidal harmonic constants. Subsequently the computed amplitude and phase of the M_2 elevation from the model are compared with coastal observations at various places over the Yellow Sea. The model grid points closest to these observation sites are shown in Fig. 1 as closed circles. Table 1 shows the comparison of observed and calculated amplitude and phase of the M_2 tide for these sites. It should be borne in mind that discrepancies between values from analyses of water levels at coastal stations and values obtained by Fourier analysis of time series from the model elements occur because generally coastal stations and corresponding model points are at slightly different locations, in region where the tidal constituents change considerably over a mesh element, so that a significant error results. In addition to these limitations, the harmonic constants were derived from short period observations of water level except for a few stations. Some variability of amplitude and phase of the M_2 tide for most stations exists.

Within limitations thus imposed, however it is shown that the model generally agrees well with observation to within 10% in amplitude and 10 degrees in phase with some deterioration in Gulf of Liantung and Hangzhou Bay reaching the maximum error of 30cm. Over the coarse grid region, the results were not improved from the previous shelf model (Choi, 1980) but in intermediate and fine grid region, the area of great interest as far as potential tidal power and large land reclamation development schemes are concerned, close agreement was achieved, errors being about 5% in amplitudes and 5 degrees in phases. Fig. 3(a) shows the computed coamplitude and cophase chart of the M_2 tide from the model demonstrating good agreement with existing chart (Ogura, 1933) and previous computation from the shelf model.

The coarse grid Yellow Sea model was run for 17 days to compute S_2 , K_1 and O_1 tidal distribution in addition to previously computed M_2 tide in the Yellow Sea. For this run harmonic constants for open boundary inputs were deduced from existing tidal charts by adopting the mean values of $H_s/H_{m_2} = 0.4$, $\alpha_{S_2} - \alpha_{m_2} = 38^\circ$ and $H_{o_1}/H_{k_1} = 0.7$, $\alpha_{k_1} - \alpha_{o_1} = 30^\circ$. Harmonic analyses for each of the grid elements were performed over 15

Table 1. Comparison of observed and calculated amplitude $H(m)$ and phase κ (degree referred to $135^\circ E$) for the M_2 tide.

Station	Code	Position of Station	Observed		Calculated	
			H	κ	H	κ
Lia Ho	LH	40°38'N 122°10'E	1.17	179	0.84	182
Hsinlutu	HL	40°08'N 120°12'E	0.13	237	0.13	190
Chinwangtao	CT	39°54'N 119°10'E	0.14	346	0.26	39
Tyoto	TT	39°54'N 121°40'E	0.65	62	0.60	49
Taku	TK	38°59'N 117°42'E	0.94	130	0.65	138
Sha-lei-tein tao	ST	38°56'N 118°31'E	0.60	96	0.38	114
Li Tsin Ho Bar	LB	37°53'N 118°40'E	0.40	208	0.30	175
Chimutao Kaochiao	CK	37°41'N 120°13'E	0.50	318	0.22	313
Ryozun	RZ	38°48'N 121°15'E	0.84	337	0.64	333
Nanfachen	NF	38°21'N 120°54'E	0.60	337	0.44	337
Tangluantsu	TL	37°59'N 120°41'E	0.56	321	0.37	328
Dairen	DR	38°56'N 121°39'E	0.99	327	0.75	317
Dai Tyozando	DT	39°16'N 122°35'E	1.32	305	1.13	297
Takushan	TS	39°46'N 123°33'E	1.93	295	1.33	287
Amnok R.	AR	40°07'N 124°24'E	0.87	1	0.89	1
Gado	GD	39°31'N 124°40'E	2.08	276	1.86	298
Unmudo	UI	39°25'N 125°07'E	2.22	337	2.00	304
Jinnampo	JP	38°38'N 125°00'E	1.56	250	1.50	246
Off Chefoo	A	37°57'N 121°55'E	0.74	332	0.53	324
Off Shantung	B	37°37'N 122°47'E	0.20	315	0.20	318
White Rock Point	WP	37°29'N 121°38'E	0.60	340	0.58	329
Weihaiwei	WW	37°30'N 122°10'E	0.59	341	0.50	344
Sangkau Bay	SB	37°03'N 122°29'E	0.70	72	0.48	74
Mongkeumpo	MK	38°11'N 124°47'E	1.12	222	0.95	217
Daechungdo	DC	37°50'N 124°43'E	0.99	178	0.89	185
Moodo	MD	37°44'N 125°33'E	1.98	158	1.75	164
Tau Tsui Head	TH	36°44'N 121°39'E	1.00	117	0.86	106
Star Reef	SR	36°23'N 120°50'E	1.20	150	0.95	143
Chintau	CU	36°05'N 120°19'E	1.25	174	0.95	148
Wang Chia Tai Bay	WB	35°32'N 119°45'E	1.20	183	1.12	183
Bamboo I.	BI	34°45'N 119°26'E	1.20	216	1.23	210
Sang Chia Chun	SN	32°01'N 121°42'E	1.10	4	0.17	21
Central Yellow Sea	C	35°39'N 123°45'E	0.83	86	0.66	83
Daeheuksando	DH	34°41'N 125°26'E	1.02	48	1.08	19
Chindo	CD	34°30'N 126°12'E	1.13	49	1.13	16
Jumundo	JD	37°39'N 126°14'E	2.70	157	2.71	169
Naeri	NR	37°38'N 126°23'E	2.80	159	2.83	169
Inchon	IC	37°29'N 126°37'E	2.92	148	3.00	168
Somoouido	SM	37°22'N 126°27'E	2.77	141	2.72	161
Palmido	PM	37°21'N 126°32'E	2.84	144	2.88	165
Guisan	GS	36°59'N 126°43'E	2.13	109	2.15	86
Weindo	WI	36°13'N 126°02'E	1.75	103	1.78	90
Duckjuckdo	DJ	37°15'N 126°09'E	2.48	140	2.48	156
Soyado	SD	37°14'N 126°10'E	2.51	142	2.43	154
Youngeungdo	YH	37°15'N 126°30'E	2.78	141	2.79	157
Baegado	BA	37°04'N 125°57'E	2.20	132	2.30	139
Janggohang	JH	37°02'N 126°34'E	2.83	143	2.85	153
Asan	AS	36°58'N 126°47'E	3.03	144	3.09	166
Dugampo	DP	36°58'N 126°31'E	2.69	138	2.78	154
Umoodo	UM	37°02'N 126°27'E	2.62	136	2.62	151
Garolim	GR	36°57'N 126°19'E	2.40	135	2.56	144
Hagampo	HG	36°53'N 126°12'E	2.29	126	2.31	127
Chonsu Bay	CB	36°23'N 126°26'E	2.26	115	2.21	119

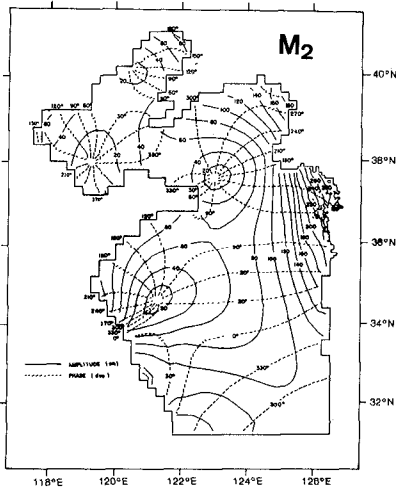


Fig. 3(a)

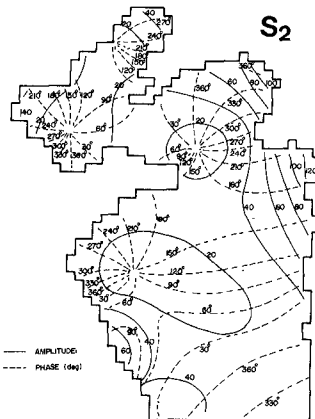


Fig. 3(b)

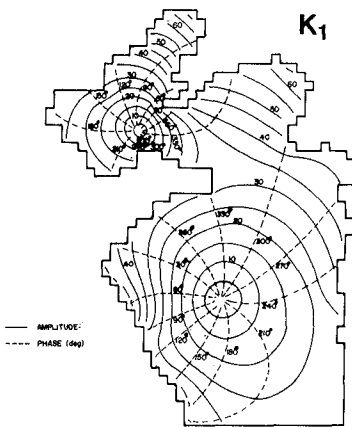


Fig. 3(c)

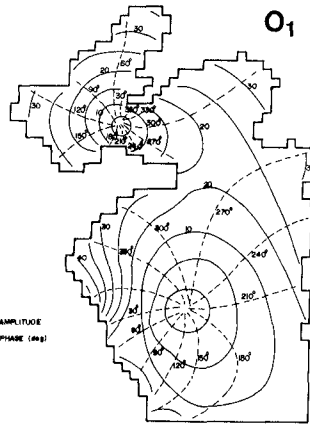


Fig. 3(d)

Fig. 3. Computed M₂, S₂, K₁ and O₁ tides from the model.

days of hourly data after discarding the first two days of data containing initial disturbances. Subsequently computed tidal charts of S_2 , K_1 and O_1 tides are drawn as shown in Fig. 3(b) - 3(d). Comparison between observations and model results showed that amplitude of S_2 tide overestimated up to 30% and errors in phases of K_1 and O_1 tides were order of 10 degrees. Overall the model gave general qualitative and quantitative agreement with the existing charts and shore-based data when the crudeness of open boundary tidal data is considered.

Tidal Currents

Fig. 4 show an example of computed tidal current fields from the dynamically linkaged model at the time of lunar transit across 135°E . It can be seen from this figure that tidal currents are very strong along the coast of Taean Peninsula and to approach channel to Incheon and Asan. Sets of current vectors also undergo harmonic oscillations of tidal period, - thus the resultant velocity vectors describing the M_2 tidal ellipses are shown in Fig. 5. This chart gives an overall impression of the magnitude and direction of the M_2 tidal current distribution representing the maximum and minimum velocities as major and minor axes respectively. It is worth noting that rotating current pattern in the lower part of the Yellow Sea is in good agreement with Ogura's speculation. In near-coastal areas, elongated major axes indicates current is near-rectilinear.

In Fig. 6 the depth-mean M_2 current ellipses are plotted for the 27 stations over the Kyonggi Bay. The magnitude and time of occurrence of the maximum M_2 tidal currents, at various places are indicated in this plot. Highest currents calculated are of the order of 150 cm/sec in this area. Current observations of comparable quality do not exist over this region, but generally good agreement of the current magnitude can be expected from the fact that the model simulates the M_2 surface elevation over this region with good accuracy.

Computed depth-mean tidal currents from the extended run of coarse grid model were also harmonically analyzed to provide harmonic constants of easterly and northerly components of S_2 , K_1 and O_1 tidal currents. This computed result was then compared with current observations from USA - China Marine Sedimentation Dynamics Study (shown as stations M2, M5; refer Larsen et al., 1985), LSU moored current meter data during 1982 experiment and WHOI moored current meter data during November, 1983 and USA - Korea cooperative current observations during 1986 (shown as stations B, D, F, I in Fig. 1).

Fig. 7 and Fig. 8 show comparison between observations and computed currents of M_2 , K_1 tides in the form of tidal ellipses which was constructed from harmonic constants. In these figures observed ellipses are shown as solid lines and computed ellipses dotted lines. There is inherent limitation in direct comparison between observed current meter data which was measured at certain depths below sea surface and depth-averaged currents computed from the two-dimensional model, however there is general agreement between the observations and model results.

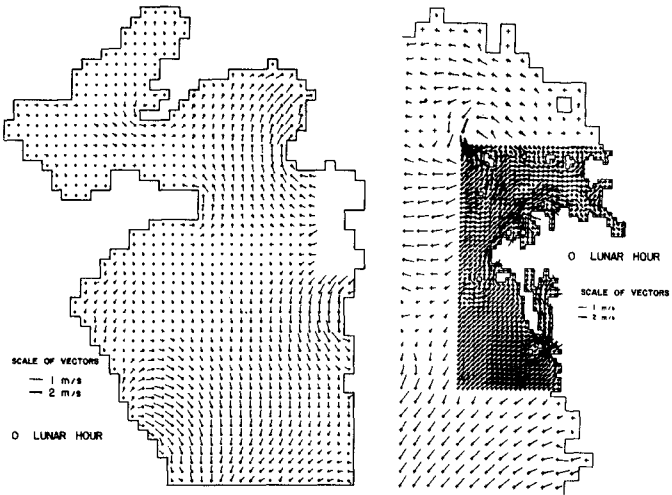


Fig. 4. Computed depth-mean M_2 tidal current from the model.

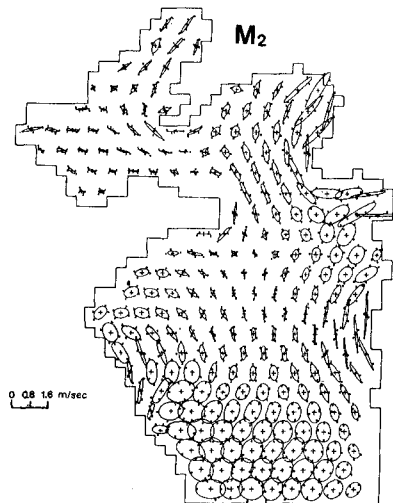


Fig. 5. Computed M_2 tidal ellipses in the Yellow Sea.

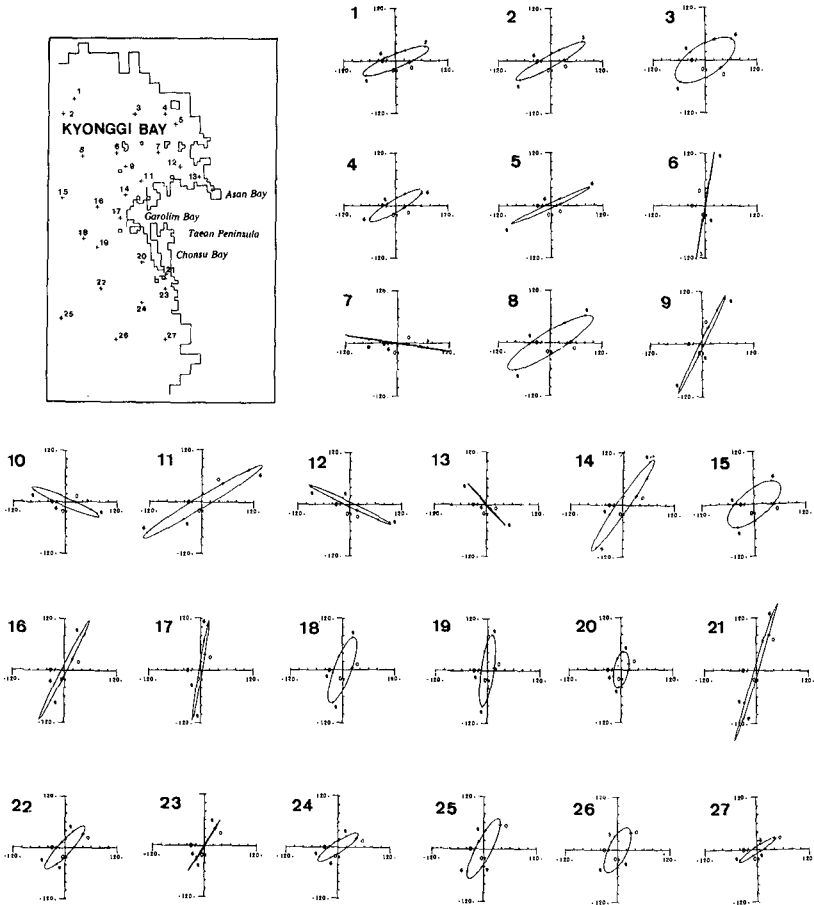


Fig. 6. Computed M_2 tidal ellipses in Kyonggi Bay.

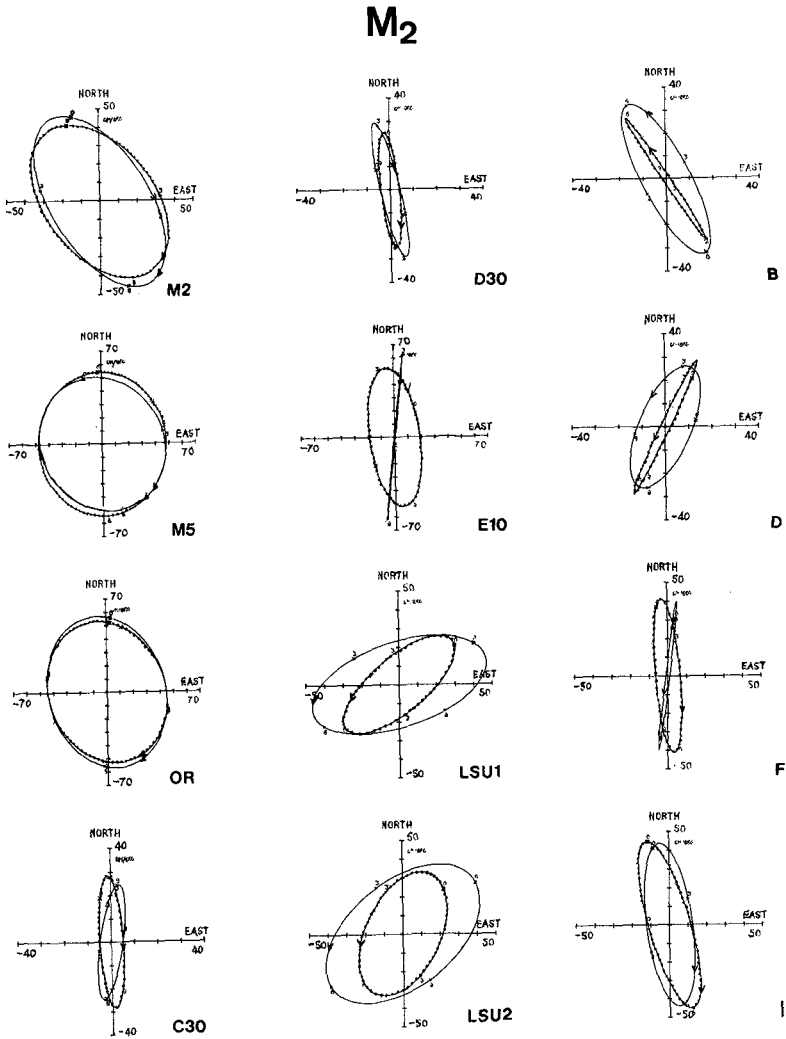


Fig. 7. Comparison of M₂ tidal ellipses between observed currents (—) and computed currents (.....). Stations WHOI 1,2,3 are shown as E,D,C.

K₁

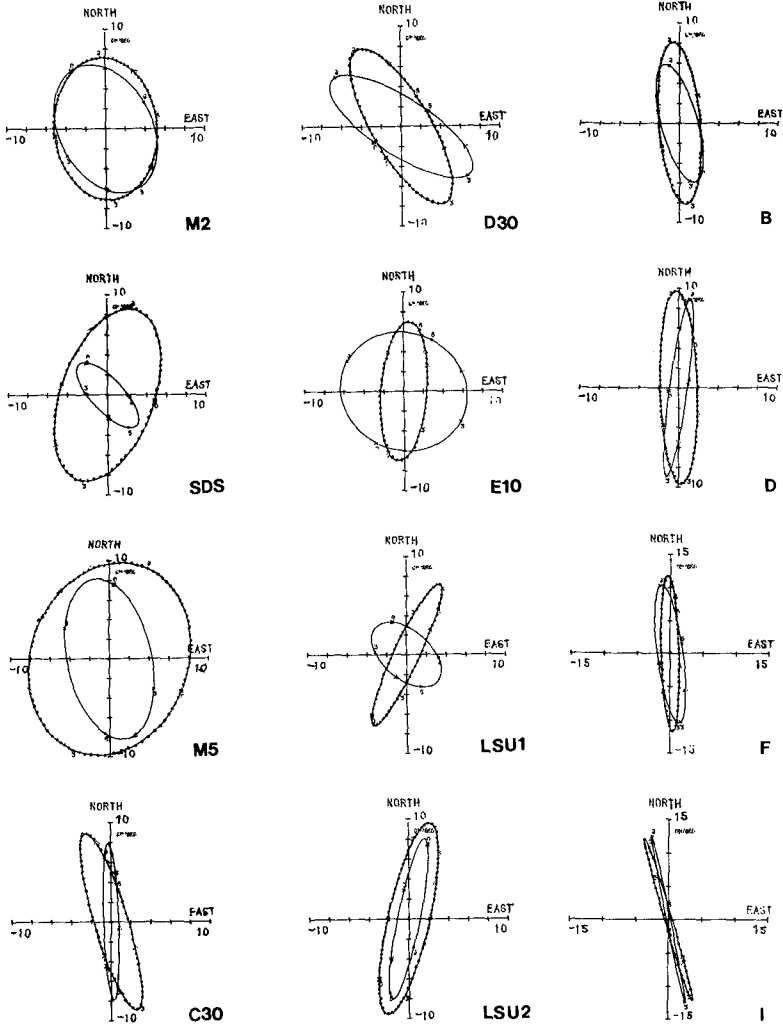


Fig. 8. Comparison of K_1 tidal ellipses between observed currents (—) and computed currents (.....). Stations WHOI 1,2,3 are shown as E,D,C.

Conclusion

Some of preliminary results from a non-linear two-dimensional model of the Yellow Sea have been presented in this paper.

The overall tidal regime of major tidal constituents in the Yellow Sea has been computed quite successfully with the coarse grid numerical model employed here. Using this coarser mesh shelf model to provide boundary data for finer mesh models in the western Yellow Sea, the near-shore variations in tides within Kyonggi Bay will be modelled in detail.

A model employing a dynamical grid nesting procedure to give fine resolution on the west coast of Korea could satisfactorily reproduced the M_2 tide in the fine mesh region in detailed manner. By this means tidal modification due to large development schemes can be evaluated.

Acknowledgements

Modelling work described here was initiated during my visit to Bidston Observatory. The author is indebted to scientists in the dynamic modelling group of Bidston Observatory. The author also wishes to thank Dr. L. H. Larsen, University of Washington, Dr. R. C. Beardsley, WHOI and Dr. J. T. Wells, South Carolina State University for making the current meter data available. Funding for this work was partially provided by Korea Science and Engineering Foundation.

References

- An, H. S. (1977). A numerical experiment of the M_2 tide in the Yellow Sea. *Journal of the Oceanographical Society of Japan*, Vol. 33, pp. 103-110.
- Boris, L. I. (1958). Calculation of the tides and tidal currents in the Yellow Sea. *Trudy Leningrad Gridromet Inst.*
- Choi, B. H. (1980). A tidal model of the Yellow Sea and the Eastern China Sea. *Korea Ocean Research and Development Institute Report 80-02.*
- Flather, R. A. (1976). A tidal model of the North-West European continental shelf. *Memoires de la Societe Royale des Sciences de Liege, Ser. 6*, Vol. 10, pp. 141-164.
- Flather, R. A. and Heaps, N. S. (1975). Tidal computations for Morecambe Bay. *Geophysical Journal of the Royal Astronomical Society*, Vol. 42, pp. 489-517.
- Larsen, L. H., Cannon, G. A. and Choi, B. H. (1985). East China Sea tide current. *Continental Shelf Research*, Vol. 4, Nos 1/2, pp. 77-103.
- Ogura, S. (1933). The tides in the seas adjacent to Japan. *Bulletin of Hydrographic Department, Imperial Japanese Navy*, No. 7, pp. 1-189.

- Owen, A. (1979). Tides in Bristol Channel: tidal barrage studies. Ph.D. thesis, University of Liverpool.
- Roberts, K. V. and Weiss, N. O. (1967). Convective difference schemes. *Math. Comput.*, Vol. 20, pp. 272-299.
- Shen, Y. (1980). Numerical computation of tides in the East China Sea. *Journal of Shandong College of Oceanology*, Vol. 10, No. 3, pp. 26-35.
- Stepanov, S. I. and Boris, L. I. (1964). On the effect of errors in the original data on the accuracy of the solution of boundary value problems of tidal equations. *Trudy Leningrad Gridromet Inst.*, Rep. No, 17.
- Tsiklauri, I. D. and Boris, L. I. (1961). An experiment to calculate tidal phenomena by means of "URAL-1" digital computer. *Trudy Leningrad Gridromet Inst.*, Rep. No. 10.
- Xia, Z. and Wang, Z. (1984). A numerical model of the M_2 constituent in the Huanghai Sea. *Journal of Oceanography of Hunghai and Bohai Seas*, Vol. 2, No. 1.